Intercomparison of the GOS approach, superposition T-matrix method, and laboratory measurements for black carbon optical properties during aging

Cenlin He[1], Yoshi Takano[1], Kuo-Nan Liou[1], Ping Yang[2], Qinbin Li[1], and Daniel W. Mackowski[3]

[1]Department of Atmospheric and Oceanic Sciences and Joint Institute for Earth System Science and Engineering, University of California, Los Angeles, CA 90095, USA
[2]Department of Atmospheric Sciences, Texas A&M, College Station, TX 77845, USA
[3]Department of Mechanical Engineering, Auburn University, Auburn, AL 36849, USA

Correspondence to: Cenlin He (cenlinhe@atmos.ucla.edu)

Abstract

We perform a comprehensive intercomparison of the geometric-optics surface-wave (GOS) approach, the superposition T-matrix method, and laboratory measurements for optical properties of fresh and coated/aged black carbon (BC) particles with complex structures. GOS and T-matrix calculations capture the measured optical (i.e., extinction, absorption, and scattering) cross sections of fresh BC aggregates, with 5–20% differences depending on particle size. We find that the T-matrix results tend to be lower than the measurements, due to uncertainty in theoretical approximations of realistic BC structures, particle property measurements, and numerical computations in the method. On the contrary, the GOS results are higher than the measurements (hence the T-matrix results) for BC radii < 100 nm, because of computational uncertainty for small particles, while the discrepancy substantially reduces to 10% for radii > 100 nm. We find good agreement (differences < 5%) between the two methods in asymmetry factors for various BC sizes and aggregating structures. For aged BC particles coated with sulfuric acid, GOS and T-matrix results closely match laboratory measurements of optical cross sections. Sensitivity calculations show that differences between the two methods in optical cross sections vary with coating structures for radii < 100 nm, while differences decrease to ~10% for radii > 100 nm. We find small deviations (≤ 10%) in asymmetry factors computed from the two methods for most BC coating structures and sizes, but several complex structures have 10–30% differences. This

© 2016. This manuscript version is made available under the Elsevier user license
http://www.elsevier.com/open-access/userlicense/1.0/

study provides the foundation for downstream application of the GOS approach in radiative transfer and climate studies.

Keywords

Black carbon, GOS, T-matrix, Optical property, BC aging, BC morphology

1. Introduction

Black carbon (BC) is the most important light-absorbing aerosol in the current atmosphere because of its strong positive climate forcing from direct radiative and snow albedo effects [*Ramanathan and Carmichael*, 2008; *Bond et al.*, 2013]. Both effects are significantly affected by BC optical properties during atmospheric aging [*Bond et al.*, 2013; *He et al.*, 2014], which transforms BC from freshly emitted hydrophobic aggregates to hydrophilic particles coated with soluble materials [*Schwarz et al*., 2008; *Zhang et al.*, 2008; *He et al.*, 2016]. Observations have shown that BC particles experience considerable variations in optical properties via aging, due to complex changes in particle morphology [*Adachi et al*., 2010; *Adachi and Buseck*, 2013; *China et al*, 2015]. Thus, a reliable estimate of BC climatic effects requires accurate computations of optical properties for BC particles with complex structures during aging.

A number of theoretical approaches have been developed and are widely used to compute particle single-scattering properties, including the Lorenz-Mie (LM) method for homogeneous spheres or concentric core-shell structures [*Toon and Ackerman*, 1981], the Finite Difference Time Domain (FDTD) method for nonspherical particles [*Yang and Liou*, 1996], the Rayleigh-Debye-Gans (RDG) approximation for homogeneous fractal aggregates [*Dobbins and Megaridis*, 1991], the Discrete Dipole Approximation (DDA) [*Draine and Flatau*, 1994] and the superposition T-matrix method [*Mackowski and Mishchenko*, 1996] for inhomogeneous and irregular shapes. Particularly, the superposition T-matrix method has increasing popularity due to its ability to deal with various aggregating structures with high accuracy [*Mackowski*, 2014]. For example, *Liu and Mishchenko* [2007] and *Liu et al*. [2008] used the superposition T-matrix method to compute radiative properties of BC aggregates with different compactness and sizes. *Kahnert and Devasthale* [2011] quantified the morphological effects of fresh BC aggregates on optical properties based on the T-matrix calculation. *Mishchenko et al.* [2014] applied the T-matrix method to study optical properties of BC-cloud mixtures.

Recently, *Liou et al*. [2010, 2011] developed a geometric-optics surface-wave (GOS) approach to compute particle light absorption and scattering by explicitly resolving complex particle structures. They found that optical cross sections, single scattering albedos, and asymmetry factors of particles calculated from the GOS method are consistent (differences < 20%) with

those derived from the LM method for concentric core-shell particles [*Liou et al*., 2010], the DDA and FDTD methods for plate and column ice crystals [*Liou et al.*, 2011], and the superposition T-matrix method for fresh BC aggregates [*Takano et al*., 2013]. Compared with the aforementioned methods, the GOS approach can be applied to a wider range of particle sizes and mixing structures with high computational efficiency. *Liou et al*. [2014] and *He et al*. [2014] applied the GOS approach to deal with multiple internal mixing of BC with nonspherical snow grains (up to 1000 μm), where the T-matrix and DDA methods currently are unsuitable. However, comprehensive evaluation and validation of the GOS approach for small and complex coated BC particles have not been performed.

He et al. [2015] compared optical cross sections of BC aggregates from GOS calculations and laboratory measurements, and found that GOS results generally captured the measurements. In this study, as an extension of their work, we perform a comprehensive intercomparison of the GOS approach, the superposition T-matrix method, and laboratory measurements for optical properties of fresh and coated BC particles with complex structures during aging. We describe the theoretical calculations and laboratory experiments in Section 2. We compare and discuss the GOS, T-matrix, and experimental results in Section 3. Finally, we present conclusions in Section 4.

2. Methods

2.1 Geometric-optics surface-wave (GOS) approach

The GOS approach [*Liou et al*., 2011, 2014; *He et al*., 2014, 2015], accounting for geometric reflection and refraction, diffraction, and surface wave components (Fig. 1a), is designed only to compute particle optical cross sections and asymmetry factors for application to radiative transfer and climate modeling. It does not compute the full Mueller matrix. The GOS approach computes particle optical properties by explicitly simulating various aggregating and coating structures. The irregular particle shapes are constructed by a stochastic procedure [*Liou et al*., 2011] in a 3-D coordinate system. Once the shape and composition of a particle are defined from the stochastic process, the geometric reflection and refraction are carried out using hit-and-miss Monte Carlo photon tracing. Following a ray-by-ray integration approach [*Yang and Liou*, 1997], the extinction and absorption cross sections for a single particle are computed by

$$C_{ext} = \frac{2\pi}{k^2}\mathrm{Re}\left[S_{11}\left(\hat{e}_0\right) + S_{22}\left(\hat{e}_0\right)\right], \tag{1}$$

$$C_{abs} = \frac{1}{2}\sum_{\gamma}\sum_{p=1}^{\infty}\exp\left(-2k\sum_{j=1}^{p-1}m_{i,j}d_j\right)\left[1-\exp\left(-2km_{i,p}d_p\right)\right]\left(t_1^2 r_1^{p-1} + t_2^2 r_2^{p-1}\right), \tag{2}$$

where C_{ext} and C_{abs} are the extinction and absorption cross sections, respectively. In Eq. (1), k is the wavenumber, *Re* denotes the real part, S_{11} and S_{22} are two diagonal elements of the scattering amplitude matrix in the forward direction, and $\hat{e}_0$ denotes the incident direction. In Eq. (2), the subscript index p (= 1, 2,…) indicates the internal localized ray, γ represents all incident rays impinging onto the sphere, $m_{i,j(or\ p)}$ represents the imaginary part of the refractive index for an inhomogeneous sphere, $d_{j(or\ p)}$ is a vector distance between two points, and $t_j^2 r_j^{p-1}(j = 1,2)$ indicates the cumulative product of Fresnel coefficients.

Subsequently, an effective geometric cross section (i.e., photon-number weighted shadow area on a plane perpendicular to the incident light) is used to compute the extinction and absorption efficiency for a group of randomly oriented aggregates [*Liou et al*., 2011]. Diffraction by randomly oriented particles with irregular shape is computed using the Babinet's principle and the effective geometric cross section [*Liou et al*., 2011]. Based on the geometric-optics components (reflection, refraction, and diffraction; hereinafter *GO*), we define a radiation pressure efficiency for nonspherical particles [*Liou et al*., 2011] as

$$Q_{pr}(GO) = Q_{ext}(GO) \quad g(GO)[Q_{ext}(GO) \quad Q_{abs}(GO)] \tag{3}$$

where Q_{pr}, Q_{ext}, and Q_{abs}, respectively, are the efficiency factors for radiation pressure (pr), extinction (ext), and absorption (abs), and $g(GO)$ is the geometric-optics asymmetry factor.

The surface-wave component of GOS accounts for the interaction of incident waves at grazing angles near the particle edge and propagating along the particle surface into shadow regions. Following the complex-angular-momentum (CAM) formulation developed by *Nussenzveig and Wiscombe* [1980], *Liou et al*. [2010] showed that a linear combination of the geometric optics component (i.e., *GO*) and the surface-wave adjustment (hereinafter *GOS*) leads to a solution that matches the exact LM theory so that

$$Q_w\left(GOS\right) = Q_w\left(GO\right) + f\,\Delta Q_w \sim Q_w\left(LM\right),\ w = ext, abs, pr, \tag{4}$$

where ΔQ_w is the surface-wave adjustment and f is a correction factor for nonsphericity of scattering particles [*Liou et al*., 2011], given by

$$f = c\left(r_v / r_a\right)^3, \tag{5}$$

where r_v and r_a are, respectively, volume and area equivalent radii of aggregates, and c (≤ 1) is an adjustment factor for aggregation. Thus, $f = 1$ for spheres ($r_v = r_a$) and $f \approx 0$ for elongated particles ($r_v << r_a$). For large particles (size parameters > ~50), the geometric optics component dominates.

Based on Eqs. (3) and (4), the GOS asymmetry factor $g(GOS)$ is computed by

$$g(GOS) = [1 \quad Q_{pr}(GOS)/Q_{ext}(GOS)]/ \quad (GOS) \tag{6}$$

where ω is the single scattering albedo. Because the CAM theory for surface-wave formulation cannot be applied to the $g(GOS)$ calculation for small inhomogeneous particles [*Nussenzveig and Wiscombe*, 1980], we use the improved geometric-optics method [*Yang and Liou*, 1996] and the ray-by-ray integration method [*Yang and Liou*, 1997] to compute $g(GOS)$ for inhomogeneously coated BC aggregates in this study. Considering the relatively large uncertainty in the Monte Carlo photon tracing for small particles, we further couple GOS with the RGD approximation to improve the computational accuracy of $g(GOS)$ for fresh BC aggregates with size parameter < 1, which has shown consistent results with the T-matrix calculation [*Takano et al*., 2013]. A comprehensive description of the GOS approach and its application is provided in *Liou and Yang* [2016].

2.2 Superposition T-matrix method

The superposition T-matrix method [*Mackowski and Mishchenko*, 1996, 2011] has recently been extended to calculate the scattering properties of multiple sphere domains with the removal of external configuration constraints [*Mackowski*, 2014]. It solves Maxwell's equations for fractal aggregates, where the scattering and extinction cross sections are given by

$$C_{sca} = \frac{\pi}{k^2} \sum_{n=1}^{L} \sum_{m=-n}^{n} \sum_{p=1}^{2} \left| a_{mnp}^0 \right|^2, \tag{7}$$

$$C_{ext} = \frac{\pi}{k^2} \sum_{n=1}^{L} \sum_{m=-n}^{n} \sum_{p=1}^{2} a_{mnp}^0 f_{mnp}^{0*}, \tag{8}$$

where f_{mnp}^{0} and a_{mnp}^{0}, respectively, are incident and scattered field coefficients expressed in

$$\mathbf{E}_{inc}(\mathbf{r}) = \sum_{n=1}^{L}\sum_{m=-n}^{n}\sum_{p=1}^{2} f_{mnp}^{0}\mathbf{N}_{mnp}^{(1)}(k\mathbf{r}), \tag{9}$$

$$\mathbf{E}_{sca}(\mathbf{r}) = \sum_{n=1}^{L_0}\sum_{m=-n}^{n}\sum_{p=1}^{2} a_{mnp}^{0}\mathbf{N}_{mnp}^{(3)}(k\mathbf{r}). \tag{10}$$

where $\mathbf{N}_{mnp}^{(1)}$ and $\mathbf{N}_{mnp}^{(3)}$ are vector spherical wave functions (VSWFs) with degree *m*, order *n*, and mode *p*. $\mathbf{E}_{inc}(\mathbf{r})$ and $\mathbf{E}_{sca}(\mathbf{r})$ are incident and scattered fields, respectively. The asymmetry factor (*g*) defined as

$$g = \frac{1}{2}\int_{0}^{} P(\theta)\sin\theta\cos\theta\, d\theta \tag{11}$$

is computed after the scattering matrix is numerically solved by the T-matrix method [*Liu and Mishchenko*, 2007]. $P(\theta)$ in Eq. (11) is the phase function (i.e., the first element of the scattering matrix). More details about the superposition T-matrix theory and formulation are provided in *Mackowski* [2014]. In this study, we use the Multi-Sphere T-Matrix (MSTM) version 3 program developed by *Mackowski* [2014] (available at www.eng.auburn.edu/users/dmckwski/scatcodes).

2.3 Laboratory experiments

He et al. [2015] compared GOS calculations with laboratory experiments for various aggregating structures of BC particles during aging. Extending their work, we apply both the GOS and superposition T-matrix methods to their experimental cases, where the experimental results are used as a reference for comparison of the two methods. The laboratory experiments measure optical cross sections at 532 nm wavelength for freshly emitted BC aggregates and aged BC particles coated with sulfuric acid through condensation of sulfuric acid vapor. Uncertainty in the measurement of optical cross sections is primarily from particle size, relative humidity, number density, and instrument calibration. The experiments also measure the density, mass, size, and fractal dimension of BC aggregates and coating materials, which are used as input for theoretical calculations by the GOS and T-matrix methods (see Section 2.4). Details about laboratory experiments are provided in *He et al*. [2015]. We investigate three experimental cases, where the

183 volume-equivalent radii are 41, 56, and 65 nm for fresh BC aggregates, and 49, 69, and 80 nm
184 for coated BC particles with coating thicknesses of 8, 13, and 15 nm, respectively.
185
186 **2.4 Theoretical computations**
187 We apply the GOS and superposition T-matrix methods to compute optical cross sections and
188 asymmetry factors of fresh and coated/aged BC particles at 532 nm wavelength for comparison
189 with experimental measurements (see Section 2.3). For fresh BC aggregates (Fig. 1b), the
190 standard computation case includes BC volume-equivalent radii of 41, 56, 65, and 137 nm,
191 where the first three values are in line with the experiments and the last one represents a mean
192 observed value near combustion sources in the atmosphere [*Bond et al.*, 2006]. In the standard
193 calculation, we use the measured primary spherule radius (r_{ps}) of 7.5 nm and fractal dimension
194 (D_f) of 2.1 for BC aggregates. We use $1.95 - 0.79i$ for BC refractive index as recommended by
195 *Bond and Bergstrom* [2006]. To investigate morphological effects, we increase the fractal
196 dimension to 2.5 and the primary spherule radius to 10 nm, respectively, in two sensitivity
197 calculations. We use $1.75 - 0.63i$ as the lower bound of BC refractive index [*Bond and*
198 *Bergstrom*, 2006] in a third sensitivity calculation to investigate the effect of refractive index.
199
200 For coated BC particles after aging, the pure BC component has the same volume-equivalent
201 radii (i.e., 41, 56, 65, and 137 nm) as the fresh BC aggregates, while the coating thicknesses
202 (sulfuric acid) are 8, 13, 15, and 27 nm, respectively, in the concentric core-shell structure shown
203 in Fig.1b. The first three coating thicknesses are derived from the experimental measurements
204 [*He et al.*, 2015], while the last one is set to have the same core-shell ratio as the experimental
205 case. The amounts of BC and coating material in each case are fixed for all the particle structures
206 considered in this study. We use $1.95 - 0.79i$ and $1.52 - 0i$ for the refractive indices of pure BC
207 and sulfuric acid (coating), respectively. We conduct computations for six typical coated BC
208 structures (Fig. 1b), including concentric core-shell, off-center core-shell, open-cell, closed-cell,
209 partially encapsulated, and externally attached structures based on atmospheric observations
210 [*China et al.*, 2015; *He et al.*, 2015]. We note that these structures are a simplification of coated
211 BC particles in the real atmosphere and hence may not capture all observed particle features.
212 More realistic structures such as nonspherical coating shells will be investigated in future work.
213 The BC particle structures are constructed by the stochastic procedure developed by *Liou et al.*

[2011] with a single realization for each structure, which may introduce some uncertainty. We apply the GOS and T-matrix methods to the same realization of each structure. Detailed descriptions of particle construction are provided in *He et al*. [2015].

3. Results and discussions

3.1 Fresh BC aggregates

Figures 2 and 3 show the extinction and absorption cross sections of fresh BC aggregates computed from the GOS and superposition T-matrix methods and measured from laboratory experiments. The scattering cross sections (not shown) are the differences between extinction and absorption cross sections. The standard GOS and T-matrix calculations capture the measured BC optical cross sections, with differences of 5–20% depending on BC size (Figs. 2a and 3a). However, the GOS results tend to be higher than the measurements, while the T-matrix results tend to be lower. The differences between the T-matrix and experimental results are likely caused by uncertainty associated with theoretical approximation of the complex BC structures produced by the experiments and the application of a single realization for each aggregate [*Skorupski et al.*, 2013; *Wu et al.*, 2015a, b, 2016]. Using different realizations of each structure, we found only small (< 5%) variations in optical cross sections and asymmetry factors. In addition, measurement uncertainties in particle fractal dimension and primary spherule radius could lead to the theory-measurement discrepancy. We found that increasing the fractal dimension or primary spherule radius reduces the difference between the T-matrix and experimental results in BC optical cross sections (Figs. 2c–d and 3c–d). The uncertainty involved in BC refractive index, measured optical cross sections, and numerical computations may also contribute to the discrepancy between the T-matrix results and measurements.

BC extinction, absorption, and scattering cross sections computed from the GOS approach are consistently higher than the T-matrix method for BC size (i.e., volume-equivalent radius) less than 100 nm (Figs. 2 and 3). This is because of uncertainty in the Monte Carlo photon tracing and the ray-by-ray integration for small particles. Increasing the BC radius to 137 nm reduces the difference in optical cross sections to 10%. We note that most BC particles observed in the real atmosphere are larger than 100 nm [*Bond et al*., 2006; *Schwarz et al*., 2008]. Considering the performance of the Monte Carlo photon tracing depends on the number of rays used, we doubled

the photon number and found only small (< 5%) changes in optical cross sections, suggesting a sufficient photon number in the current computations.

Similar to the T-matrix calculations, the GOS results show a 20% decrease in extinction and absorption cross sections and 30% in scattering cross sections by using the lower bound of BC refractive index ($1.75 - 0.63i$). *Liu et al*. [2008] found 50–70% differences in BC absorption and scattering cross sections by using $2 - i$ and $1.75 - 0.5i$ for refractive index, which depends on aggregate structures. By increasing the fractal dimension (from 2.1 to 2.5), we found that BC absorption cross sections computed from the GOS method decrease by 5–15% with larger reductions for larger sizes (Fig. 3c), while the T-matrix results show a rather small (< 3%) change in absorption. *Scarnato et al*. [2013] showed that more compact structures (i.e., larger fractal dimension) lead to weaker BC absorption by using the DDA method. This is because of fewer BC primary spherules directly exposed to incident rays for aggregates with a larger fractal dimension [*Liu et al*., 2008]. Both GOS and T-matrix calculations show less than 5% changes in BC extinction and absorption cross sections by increasing the primary spherule radius (Fig. 3d). This is consistent with the conclusion from *Liu and Mishchenko* [2007] that BC scattering and absorption are weakly affected by primary spherule size.

Figure 4 shows the asymmetry factor of fresh BC aggregates computed from the GOS and T-matrix methods. The GOS results closely match (differences < 5%) the T-matrix calculations for different BC sizes in both standard and sensitivity cases. The two methods show negligible (< 1%) changes in asymmetry factors when using a smaller BC refractive index. We found a 5–15% reduction in asymmetry factors for a larger primary spherule radius (r_{ps} = 10 nm) but a much stronger reduction (40–50%) for a larger fractal dimension (D_f = 2.5) for BC radii smaller than 100 nm. *Liu et al*. [2008] also showed that the asymmetry factor of BC aggregates decreases substantially with an increasing fractal dimension from 2 to 3.

3.2 Coated/aged BC particles

Figures 5 and 6 show the extinction and absorption cross sections of coated/aged BC particles computed from the GOS and superposition T-matrix methods and measured from laboratory experiments. Both GOS and T-matrix results are consistent with measurements in optical cross

sections for the concentric core-shell structure, with differences of 5–20% depending on BC size. This is consistent with the observed efficient structure compaction during BC aging in the experiments [*He et al.*, 2015]. For the concentric core-shell, off-center core-shell, and partially encapsulated structures, the GOS calculations show a good agreement with the T-matrix results in BC optical cross sections, while the GOS calculations are consistently higher than the T-matrix results for closed-cell, open-cell, and externally attached structures with radii smaller than 100 nm. The discrepancy is larger for smaller BC sizes, due to the uncertainty in the GOS calculation for small particles. As the particle radius increases to larger than 100 nm, the discrepancy between the two methods in optical cross sections reduces to less than 15% for all six coating structures.

We found that the off-center core-shell structure only leads to less than 5% change in BC optical cross sections computed from the GOS and T-matrix methods (Figs. 5 and 6), due to the small coating thickness. *He et al.* [2015] found up to 30% decrease in BC optical cross sections for the off-center core-shell structure with a thick coating layer. Similar reductions in absorption caused by the off-center position of BC cores are also found by *Adachi et al*. [2010] using the DDA method. The GOS and T-matrix results both show a substantial decrease in extinction, absorption, and scattering cross sections for the partially encapsulated structure with radii smaller than 100 nm but a slight increase for radii larger than 100 nm, relative to the concentric core-shell structure. *Kahnert et al*. [2013] pointed out that the effect of encapsulated structures on BC absorption and scattering are strongly dependent on particle size. The GOS method shows an enhancement of 40–70% in BC absorption for the closed-cell structure with radius smaller than 100 nm compared with the concentric core-shell structure, whereas the T-matrix method shows a 40% decrease in this case (Fig. 6). We note that BC absorption for the closed-cell structure, which depends on particle size and refractive index, could vary from lower to higher than that of the concentric core-shell structure. For the open-cell and externally attached structures with radii smaller than 100 nm, the T-matrix calculations lead to about 40% reduction in BC absorption relative to the concentric core-shell structure. This is likely because the two coating structures are relatively loose and open, which cannot produce effective lensing effects to enhance BC absorption [*He et al*., 2015], as well as due to the shadowing effect from non-absorbing coating material attached outside pure BC spherules [*Liu and Mishchenko*, 2007]. However, the GOS

approach shows a slight increase (≤ 15%) in BC absorption by the open-cell and externally attached structures, as a result of the overestimate produced by GOS calculations for small particles with complex structures.

Figure 7 shows the asymmetry factor of coated BC structures computed from the GOS and T-matrix methods. The T-matrix calculations show a negligible change in asymmetry factors of the off-center core-shell structure compared to the concentric core-shell structure, while the closed-cell structure results in a 10–40% increase. We found that the asymmetry factors computed from the T-matrix method for the open-cell, partially encapsulated, and externally attached structures are lower than the concentric core-shell structure with the smallest radius (i.e., 49 nm), but increase quickly to be higher than that of the concentric core-shell structure as BC size becomes larger. The GOS results generally capture the T-matrix results, but the consistency between the two methods varies across different structures and sizes. The two methods show negligible differences (≤ 5%) for concentric core-shell, off-center core-shell, and open-cell structures with all four particle sizes. The GOS calculations also agree with the T-matrix results for the externally attached structures with differences ≤ 10%. The discrepancies between the GOS and T-matrix methods are less than 10% for the closed-cell structure with radii of 49, 69, and 164 nm but reach up to 25% for a radius of 80 nm. The differences in the partially encapsulated structure also vary with size, where the GOS results show 10–30% overestimates for radii smaller than 100 nm and 15% underestimates for radii larger than 100 nm, compared with the T-matrix calculations. This is probably because of the approximation in GOS computations of asymmetry factors by the improved geometric-optics and ray-by-ray integration methods.

In addition, we compared the computational efficiency of the GOS and superposition T-matrix methods. The T-matrix calculation is usually fast for particles with size parameter less than 10, particularly when considering that orientation-averaging is done analytically. For simple particle shapes, the T-matrix method shows similar computational time as the GOS approach. However, when particles have rather complex structures such as coated BC aggregates in this study, the T-matrix calculation requires much more time than the GOS calculation. For example, for open-cell and closed-cell coating structures with radii of 164 nm, the GOS computation time is ~1 minute, whereas the T-matrix computation requires 1–2 hours.

4. Conclusions

We have performed a comprehensive intercomparison of the GOS and superposition T-matrix calculations with laboratory measurements for optical properties of fresh and coated/aged BC particles with complex structures. The GOS and T-matrix results both captured the measured optical (extinction, absorption, and scattering) cross sections of fresh BC aggregates, with differences of 5–30% depending on size. However, the T-matrix calculations tended to be lower than the measurements, due to uncertainty associated with theoretical approximations of realistic BC structures, measurements of particle properties, and numerical computations in the method. In contrast, the GOS calculations were consistently higher than the measurements (hence the T-matrix results) for BC radius smaller than 100 nm, due to computational uncertainty for small particles. The discrepancy reduced to 10% as the particle size increased to larger than 100 nm. The asymmetry factor computed from the GOS approach showed a good agreement (differences $< 5\%$) with the T-matrix results for various BC sizes and aggregating structures. Both the GOS and T-matrix results showed a 20–30% decrease in optical cross sections of fresh BC aggregates by using the lower bound of BC refractive index and less than 5% changes by increasing the primary spherule radius, while the two methods differed to some extent in the sensitivity of BC absorption to fractal dimension.

For coated/aged BC particles, the GOS and T-matrix results were consistent with laboratory measurements in optical cross sections for the concentric core-shell structure, because of the observed efficient structure compaction during BC aging. The GOS calculations showed a good agreement in optical cross sections with the T-matrix results for the concentric core-shell, off-center core-shell, and partially encapsulated structures, but were higher than the T-matrix results for the closed-cell, open-cell, and externally attached structures with radii smaller than 100 nm. The discrepancy decreased significantly for BC radii larger than 100 nm. The GOS results captured (differences $\leq 10\%$) the T-matrix calculations of asymmetry factors for different coating structures and sizes, except for a few particle sizes of the closed-cell and partially encapsulated structures. We found that the sensitivity of optical cross sections and asymmetry factors to BC coating strongly depends on particle structures and sizes, where the GOS results deviated to some extent from the T-matrix calculations. This is likely due to uncertainty in GOS

calculations for small particles with complex structures. This study provided the foundation to further apply the GOS approach to radiative transfer and climate studies in future work.

Acknowledgements

We thank the reviewers for their helpful comments and suggestions. This research was supported by the NSF [EAGER grant AGS-1523296].

References

Adachi, K., and P. R. Buseck (2013), Changes of ns-soot mixing states and shapes in an urban area during CalNex, *J. Geophys. Res.-Atmos.*, *118*(9), 3723-3730, doi:10.1002/Jgrd.50321.

Adachi, K., S. H. Chung, and P. R. Buseck (2010), Shapes of soot aerosol particles and implications for their effects on climate, *J. Geophys. Res.-Atmos.*, *115*, D15206, doi:10.1029/2009jd012868.

Bond, T. C., and R. W. Bergstrom (2006), Light absorption by carbonaceous particles: An investigative review, *Aerosol Sci. Tech.*, *40*(1), 27-67, doi:10.1080/02786820500421521.

Bond, T. C., G. Habib, and R. W. Bergstrom (2006), Limitations in the enhancement of visible light absorption due to mixing state, *J. Geophys. Res.*, *111*, D20211, doi:10.1029/2006JD007315.

Bond, T. C., et al. (2013), Bounding the role of black carbon in the climate system: A scientific assessment, *J. Geophys. Res. Atmos.*, *118*, 5380–5552, doi:10.1002/jgrd.50171.

China, S., et al. (2015), Morphology and mixing state of aged soot particles at a remote marine free troposphere site: Implications for optical properties, *Geophys. Res. Lett.*, 42, doi:10.1002/2014GL062404.

Dobbins, R. A., and C. M. Megaridis (1991), Absorption and Scattering of Light by Polydisperse Aggregates, *Appl. Optics*, *30*(33), 4747-4754.

Draine, B. T., and P. J. Flatau (1994), Discrete-Dipole Approximation for Scattering Calculations, *J. Opt. Soc. Am. A*, *11*(4), 1491-1499, doi:10.1364/Josaa.11.001491.

He, C., Q. Li, K.-N. Liou, Y. Takano, Y. Gu, L. Qi, Y. Mao, and L. R. Leung (2014), Black carbon radiative forcing over the Tibetan Plateau, *Geophys. Res. Lett.*, *41*, 7806–7813, doi:10.1002/2014GL062191.

He, C., K. N. Liou, Y. Takano, R. Zhang, M. L. Zamora, P. Yang, Q. Li, and L. R. Leung (2015), Variation of the radiative properties during black carbon aging: theoretical and experimental intercomparison, *Atmos. Chem. Phys.*, *15*(20), 11967-11980, doi:10.5194/acp-15-11967-2015.

He, C., Q. Li, K. -N. Liou, L. Qi, S. Tao, and J. P. Schwarz (2016), Microphysics-based black carbon aging in a global CTM: constraints from HIPPO observations and implications for global black carbon budget, *Atmos. Chem. Phys.*, *16*, 3077-3098, doi:10.5194/acp-16-3077-2016.

Kahnert, M., and A. Devasthale (2011), Black carbon fractal morphology and short-wave radiative impact: a modelling study, *Atmos. Chem. Phys.*, *11*(22), 11745-11759, doi:10.5194/acp-11-11745-2011.

Kahnert, M., T. Nousiainen, and H. Lindqvist (2013), Models for integrated and differential scattering optical properties of encapsulated light absorbing carbon aggregates, *Opt. Express*, *21*(7), 7974-7993, doi:10.1364/Oe.21.007974.

Liou, K. N., Y. Takano, and P. Yang (2010), On geometric optics and surface waves for light scattering by spheres, *J. Quant. Spectrosc. Radiat. Transfer*, *111*, 1980–1989, doi:10.1016/j.jqsrt.2010.04.004.

Liou, K. N., Y. Takano, and P. Yang (2011), Light absorption and scattering by aggregates: Application to black carbon and snow grains, *J. Quant. Spectrosc. Radiat. Transfer*, *112*(10), 1581–1594, doi:10.1016/j.jqsrt.2011.03.007

Liou, K. N., Y. Takano, C. He, P. Yang, L. R. Leung, Y. Gu, and W. L. Lee (2014), Stochastic parameterization for light absorption by internally mixed BC/dust in snow grains for application to climate models, *J. Geophys. Res.-Atmos.*, *119*, 7616–7632, doi:10.1002/2014JD021665.

Liou, K. N. and P. Yang (2016), Light scattering by ice crystals: Fundamentals and applications, Cambridge University Press, Cambridge, in press.

427 Liu, L., and M. I. Mishchenko (2007), Scattering and radiative properties of complex soot and
428 soot-containing aggregate particles, *J. Quant. Spectrosc. Radiat. Transfer*, *106*(1-3), 262-
429 273, doi:10.1016/j.jqsrt.2007.01.020.
430 Liu, L., M. I. Mishchenko, and W. P. Arnott (2008), A study of radiative properties of fractal
431 soot aggregates using the superposition T-matrix method, *J. Quant. Spectrosc. Radiat.*
432 *Transfer*, *109*(15), 2656-2663, doi:10.1016/j.jqsrt.2008.05.001.
433 Mackowski, D. W. (2014), A general superposition solution for electromagnetic scattering by
434 multiple spherical domains of optically active media. *J. Quant. Spectrosc. Radiat. Transfer*,
435 *133*, 264–270.
436 Mackowski, D. W., and M. I. Mishchenko (1996), Calculation of the *T* matrix and the scattering
437 matrix for ensembles of spheres, *J. Opt. Soc. Am. A*, *13*(11), 2266-2278,
438 doi:10.1364/Josaa.13.002266.
439 Mackowski, D. W., and M. I. Mishchenko (2011), A multiple sphere T-matrix Fortran code for
440 use on parallel computer clusters, *J. Quant. Spectrosc. Radiat. Transfer*, *112*(13), 2182-2192,
441 doi:10.1016/j.jqsrt.2011.02.019.
442 Mishchenko, M. I., L. Liu, B. Cairns, and D. W. Mackowski (2014), Optics of water cloud
443 droplets mixed with black-carbon aerosols, *Opt. Lett.*, *39*(9), 2607-2610,
444 doi:10.1364/Ol.39.002607.
445 Nussenzveig, H. M., and W. J. Wiscombe (1980), Efficiency factors in Mie scattering, *Phys. Rev.*
446 *Lett.*, *45*(18), 1490-1494, doi:10.1103/PhysRevLett.45.1490.
447 Ramanathan, V., and G. Carmichael (2008), Global and regional climate changes due to black
448 carbon, *Nat. Geosci.*, *1*(4), 221–227, doi:10.1038/Ngeo156.
449 Scarnato, B. V., S. Vahidinia, D. T. Richard, and T. W. Kirchstetter (2013), Effects of internal
450 mixing and aggregate morphology on optical properties of black carbon using a discrete
451 dipole approximation model, *Atmos. Chem. Phys.*, *13*(10), 5089-5101, doi:10.5194/acp-13-
452 5089-2013.
453 Schwarz, J. P., et al. (2008), Coatings and their enhancement of black carbon light absorption in
454 the tropical atmosphere, *J. Geophys. Res.-Atmos.*, *113*(D3), D03203,
455 doi:10.1029/2007jd009042.
456 Skorupski, K., J. Mroczka, N. Riefler, H. Oltmann, S. Will, and T. Wriedt (2013), Impact of
457 morphological parameters onto simulated light scattering patterns, *J. Quant. Spectrosc.*

458 *Radiat. Transfer*, 119, 53-66, doi:10.1016/j.jqsrt.2012.12.014.
459 Takano, Y., K. N. Liou, M. Kahnert, and P. Yang (2013), The single-scattering properties of
460 black carbon aggregates determined from the geometric-optics surface-wave approach and
461 the T-matrix method, *J. Quant. Spectrosc. Radiat. Transfer*, *125*, 51-56,
462 doi:10.1016/j.jqsrt.2013.04.006.
463 Toon, O. B., and T. P. Ackerman (1981), Algorithms for the calculation of scattering by
464 stratified spheres, *Appl. Optics*, *20*(20), 3657-3660, doi:10.1364/Ao.20.003657.
465 Wu, Y., T. Cheng, L. Zheng, and H. Chen (2015a), A Study of Optical Properties of Soot
466 Aggregates Composed of Poly-Disperse Monomers Using the Superposition T-Matrix
467 Method, *Aerosol Sci. Technol.*, 49(10), 941-949, doi:10.1080/02786826.2015.1083938.
468 Wu, Y., T. Cheng, L. Zheng, H. Chen, and H. Xu (2015b), Single scattering properties of semi-
469 embedded soot morphologies with intersecting and non-intersecting surfaces of absorbing
470 spheres and non-absorbing host, *J. Quant. Spectrosc. Radiat. Transfer*, 157, 1-13,
471 doi:10.1016/j.jqsrt.2015.02.006.
472 Wu, Y., T. Cheng, L. Zheng, and H. Chen (2016), Effect of morphology on the optical properties
473 of soot aggregated with spheroidal monomers, *J. Quant. Spectrosc. Radiat. Transfer*, 168,
474 158-169, doi:10.1016/j.jqsrt.2015.09.017.
475 Yang, P., and K. N. Liou (1996), Finite-difference time domain method for light scattering by
476 small ice crystals in three-dimensional space, *J. Opt. Soc. Am. A*, *13*(10), 2072-2085,
477 doi:10.1364/Josaa.13.002072.
478 Yang, P., and K. N. Liou (1997), Light scattering by hexagonal ice crystals: solutions by a ray-
479 by-ray integration algorithm, *J. Opt. Soc. Am. A*, *14*(9), 2278-2289,
480 doi:10.1364/Josaa.14.002278.
481 Zhang, R. Y., A. F. Khalizov, J. Pagels, D. Zhang, H. X. Xue, and P. H. McMurry (2008),
482 Variability in morphology, hygroscopicity, and optical properties of soot aerosols during
483 atmospheric processing, *P. Natl. Acad. Sci. USA*, *105*(30), 10291-10296,
484 doi:10.1073/pnas.0804860105.
485

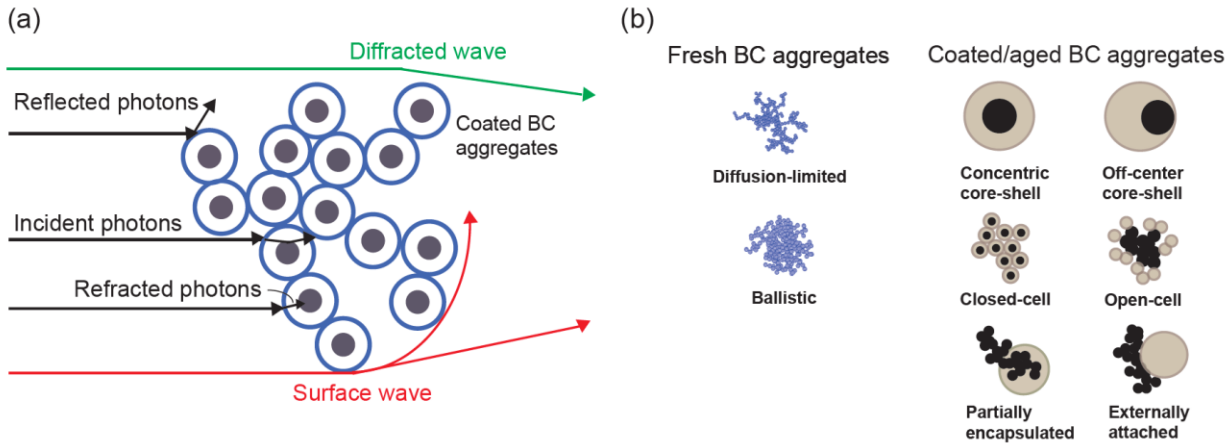

Figure 1. (a) A graphical demonstration of the geometric-optics surface-wave (GOS) method for light scattering and absorption by BC aggregates, including reflection, refraction, diffraction, and surface-wave components. (b) Typical structures of fresh and coated BC particles used in this study to approximate atmospheric observations (modified from *He et al*. [2015] and *Liou et al*. [2011]).

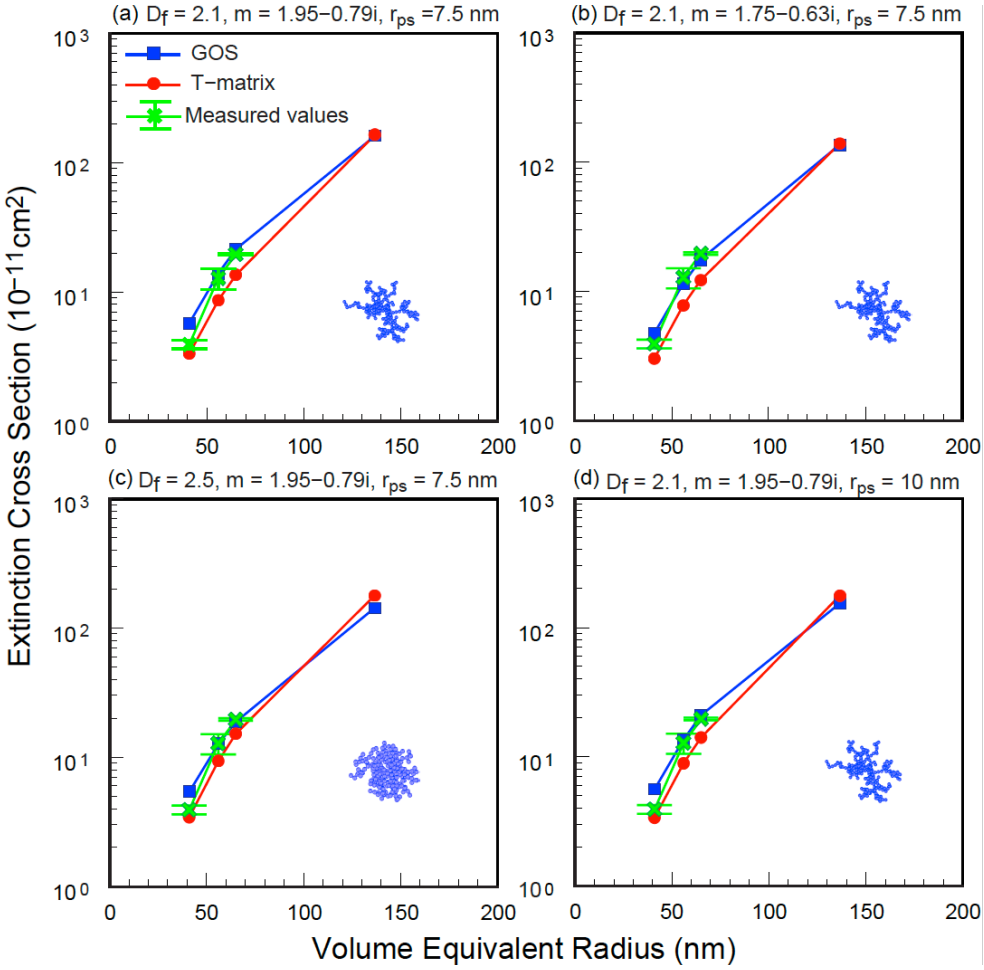

Figure 2. Extinction cross sections (at 532 nm) of fresh BC aggregates computed from the GOS (blue) and superposition T-matrix (red) methods and measured from laboratory experiments (green). One standard case (a) and three sensitivity cases (b–d) are shown with different fractal dimensions (D_f), BC refractive index (m), and radius of primary spherule (r_{ps}). Note that the measured values shown as a reference are the same in all four panels.

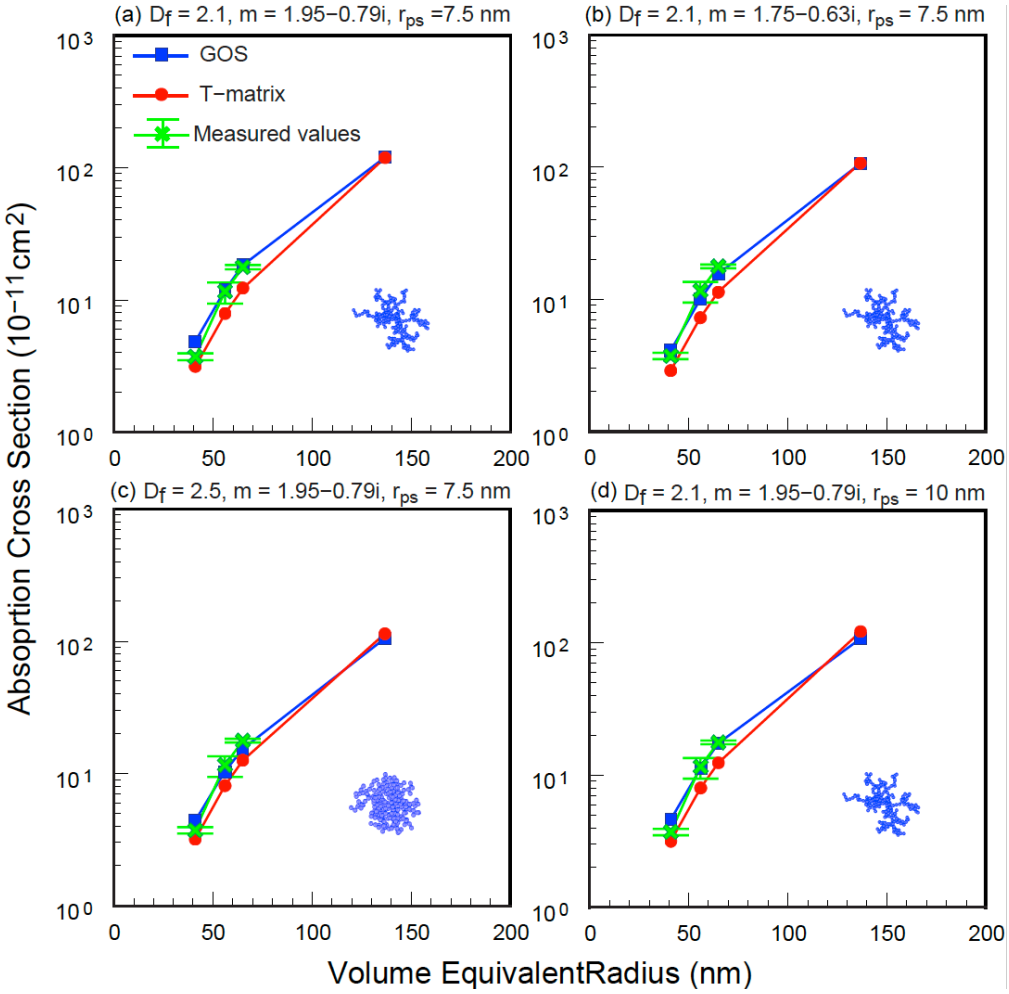

503
504

505 **Figure 3.** Same as **Figure 2**, but for absorption cross sections.

506

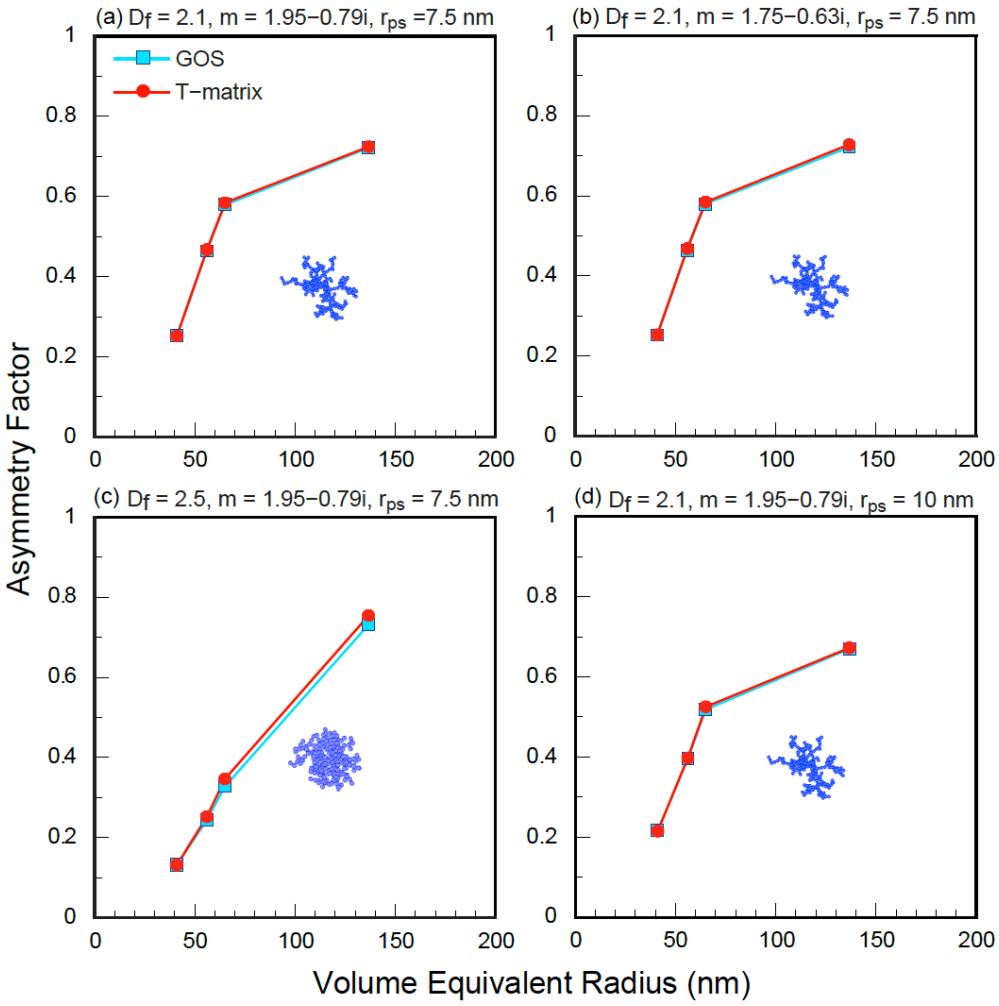

Figure 4. Same as **Figure 2**, but for asymmetry factors. Note that asymmetry factors are not measured in laboratory experiments.

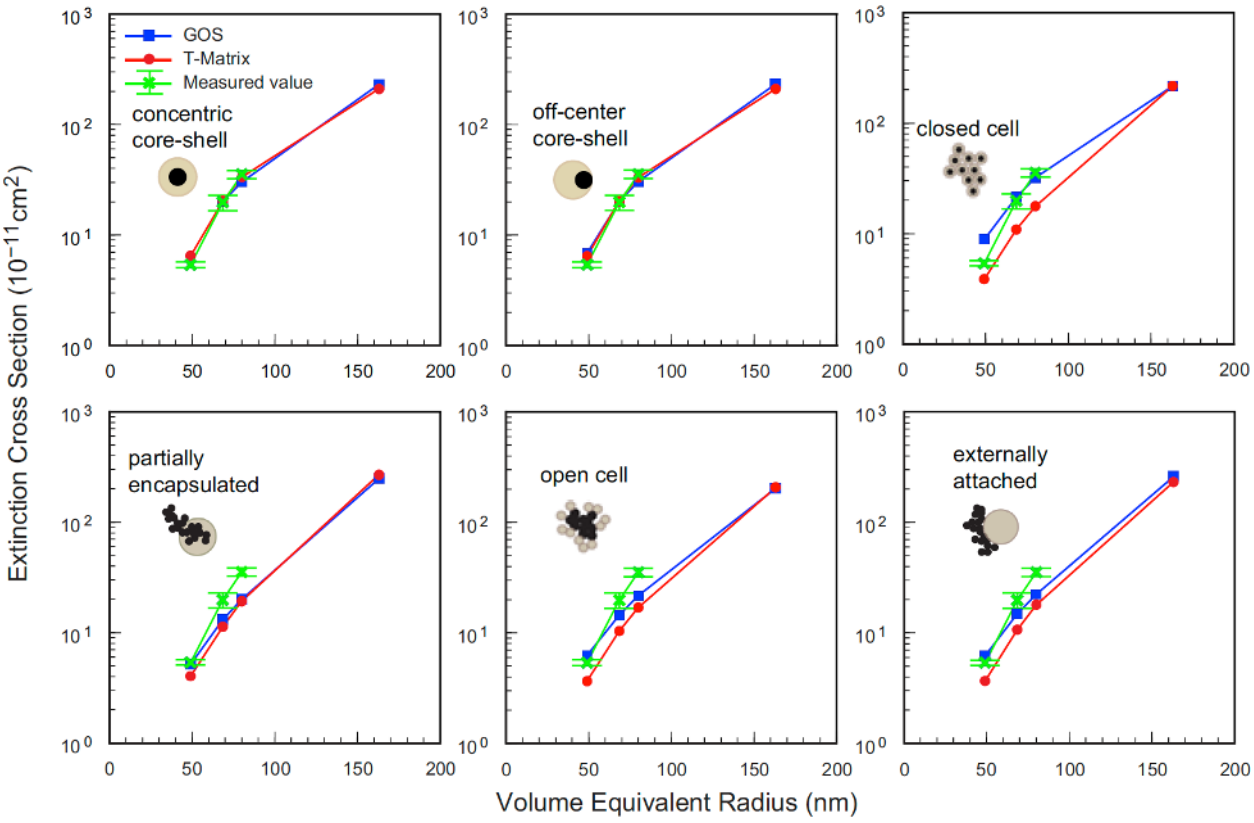

512
513

514 **Figure 5.** Extinction cross sections (at 532 nm) of coated BC particles with six typical structures
515 computed from the GOS (blue) and superposition T-matrix (red) methods and measured from
516 laboratory experiments (green). Note that the measured values shown as a reference are the same
517 in all panels.

518

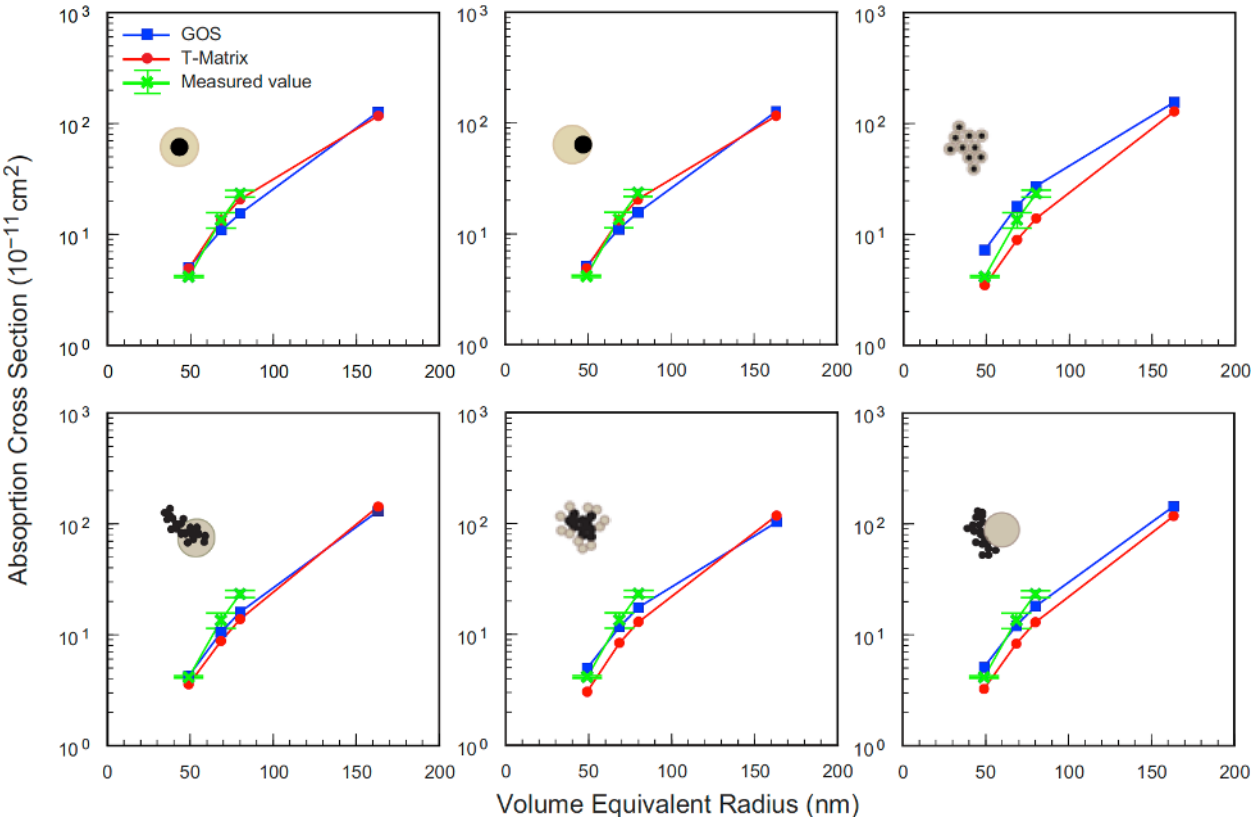

519
520

521 **Figure 6.** Same as **Figure 5**, but for absorption cross sections.

522

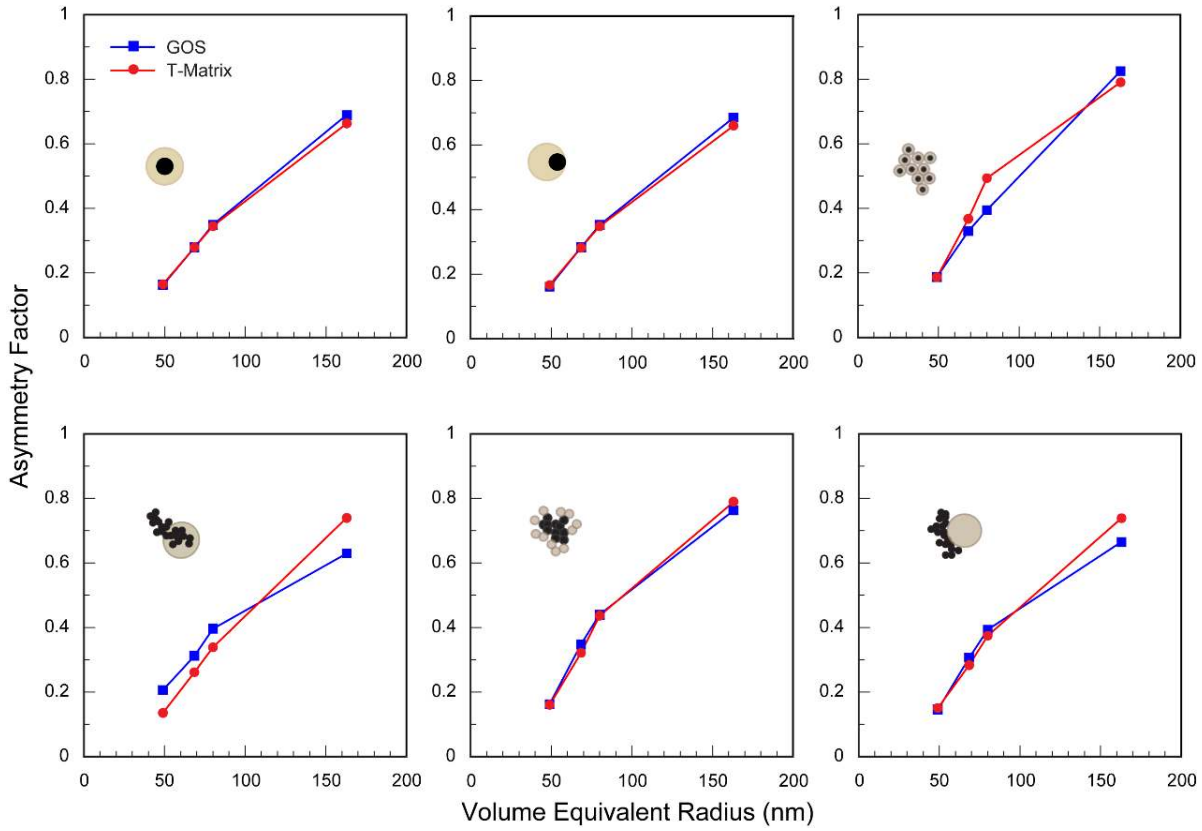

Figure 7. Same as **Figure 5**, but for asymmetry factors. Note that asymmetry factors are not measured in laboratory experiments.